ISSN 1063-7761, Journal of Experimental and Theoretical Physics, 2014, Vol. 118, No. 3, pp. 432–441. © Pleiades Publishing, Inc., 2014.
Original Russian Text © I.R. Karetnikova, K.R. Mukhamatchin, I.M. Nefedov, M.V. Sapozhnikov, A.A. Fraerman, I.A. Shereshevskii, 2014, published in Zhurnal Eksperimental'noi i Teoreticheskoi Fiziki, 2014, Vol. 145, No. 3, pp. 497–507.

ORDER, DISORDER, AND PHASE TRANSITION IN CONDENSED SYSTEM

Phase Transitions in a Two-Dimensional Dipole Ferrimagnet

I. R. Karetnikova[a,b], K. R. Mukhamatchin[b], I. M. Nefedov[a,b], M. V. Sapozhnikov[a,b,*], A. A. Fraerman[a,b], and I. A. Shereshevskii[a,b]

[a] *Institute for Physics of Microstructures, Russian Academy of Sciences, Nizhni Novgorod, 603950 Russia*
[b] *Lobachevsky State University, pr. Gagarina 23, Nizhni Novgorod, 603950 Russia*
**e-mail: msap@ipmras.ru*

Received October 21, 2013

Abstract—The magnetic configurations of the system of magnetic dipoles that have different values and are arranged in a staggered order on a square lattice are studied. A numerical simulation is used to study the phase transitions in the system when the mismatch between the dipoles changes. The restructuring of the magnetic configuration of the system induced by a change in the mismatch is shown to proceed via sequential second-order phase transitions between collinear and noncollinear phases. The numerical simulation results are supported by analytical calculations performed with trial functions.

DOI: 10.1134/S1063776114030042

1. INTRODUCTION

The character of magnetic ordering in artificial two-dimensional arrays of single-domain ferromagnetic particles, which is caused by their magnetostatic interaction, depends substantially on the type of symmetry of the lattice formed by them [1]. The magnetic properties of such systems were much studied both theoretically [1–8] and experimentally [9–14]. It is known that the ground state of a system of isotropic dipoles located on a two-dimensional lattice with an axis of symmetry higher than a diad axis is continuously degenerate at zero temperature [4, 15]. For example, the ground state of a triangular lattice is represented by the ferromagnetic ordering of dipoles that is degenerate with respect to the angle between a magnetic moment vector and the lattice axes. The ground state of a two-dimensional square lattice corresponds to a microvortex magnetization distribution, and the energy of this state is independent of the angle of inclination of the magnetic moments of dipoles to the lattice axes (Fig. 1a). The limitation imposed on the number of possible magnetic configurations of a system is caused by the fact that the magnetic moment is constant at each lattice site. Thus, only collinear and noncollinear commensurable magnetization distributions are possible in the systems formed by identical dipoles [2, 3].

The behavior of the lattices the unit cell of which contain at least two nonidentical particles is more complex. Artificial spin ice is a well-known example of such systems. This lattice is characterized by the fact that its unit cell has two magnetic particles with different easy magnetization axis directions [16]. The lattices formed by magnetic particles of various sizes represent another possible method of forming systems with a complex unit cell. In [17], we showed that an incommensurate spiral distribution of magnetic moments can exist in the one-dimensional case in such a system.

In this work, we analytically and numerically study the magnetic configurations of the two-dimensional lattices of magnetic isotropic dipoles in the case where a unit cell has two dipoles with different magnetic moments, $M^{(1)}$ and $M^{(2)}$. In essence, such a system is a two-dimensional dipole ferrimagnet. The mismatch between the magnetic moments of the sublattices is $\delta = (M^{(1)} - M^{(2)})/(M^{(1)} + M^{(2)})$. In the case where the dipoles are the same ($\delta = 0$), the energy minimum corresponds to a microvortex state on a "dense" lattice with translation vectors $\mathbf{a}_1 = (1, 0)$ and $\mathbf{a}_2 = (0, 1)$ (Figs. 1a, 2) [1, 4]. Similarly, the microvortex state is also a ground state in the case where one of the magnetic moments is zero ($\delta = 1$), and dipoles in this case are located on a "rotated" square lattice with translation vectors $\mathbf{c}_1 = (\sqrt{2}, \sqrt{2})$ and $\mathbf{c}_2 = (\sqrt{2}, -\sqrt{2})$ (Fig. 1h). In this work, we show that the transition from one distribution to another induced by a change in δ proceeds via sequential phase transitions between the collinear and noncollinear phases.

The structure of the work is as follows. In the first part, we describe a numerical model and the results of micromagnetic simulation of the magnetization distribution in the system under study. In the second part, we used the trial function method to analytically describe the phases detected in a numerical experiment and showed that the detected phase transitions are second-order phase transitions. The analytical computations are described in detail in the Appendix.

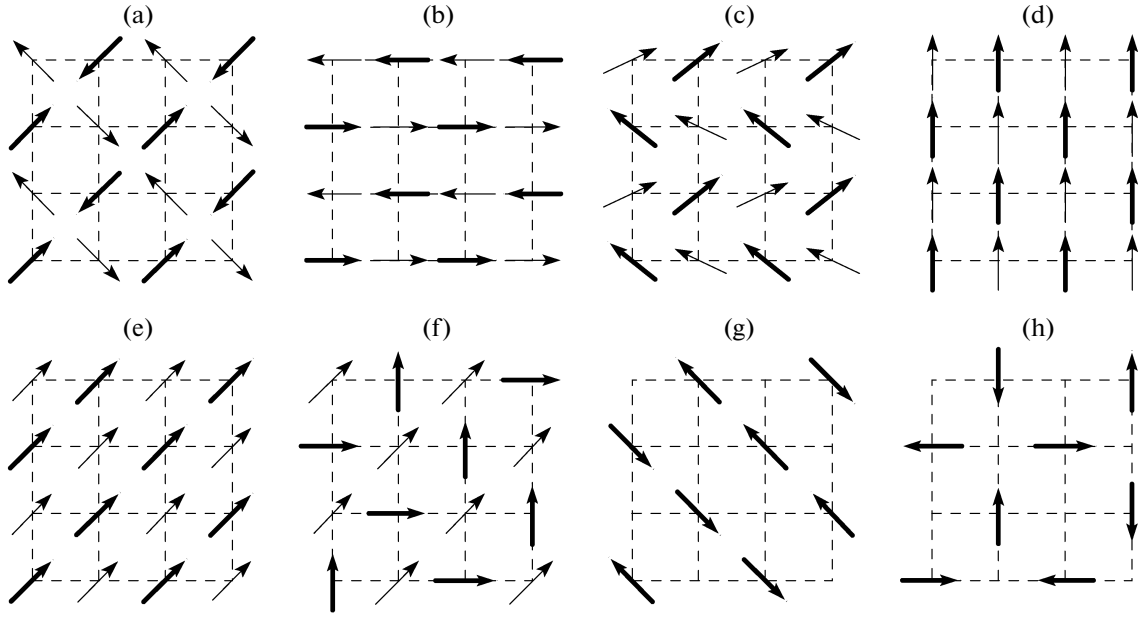

Fig. 1. Phase configurations of the system at various values of parameter δ. Heavy and thin arrows indicate large and small dipoles from the different sublattices. (a) microvortex state, $\delta = 0$, $T = 0$; (b) first antiferromagnetic state, $0 < \delta < 0.27$, $T \neq 0$; (c) noncollinear state, $0.27 < \delta < 0.45$; (d) ferromagnetic state, $0.45 < \delta < 0.673$; (e) "rotated" ferromagnetic state, $0.659 < \delta < 0.868$; (f) parquet state, $0.868 < \delta < 1$; (g) second antiferromagnetic state, $\delta = 1$, $T \neq 0$; and (h) second microvortex state, $\delta = 1$, $T = 0$.

2. SIMULATION OF THE MAGNETIC STATES OF A DIPOLE FERRIMAGNET

The system to be studied consists of two embedded square lattices of dipoles having different total magnetic moments (Fig. 2). The site coordinates of the first sublattice are designated as $\mathbf{r}_\mu^{(1)} = (\eta_x h_x, \eta_y h_y)$, where $\boldsymbol{\eta}(i, j)$ is an integer vector. The sites of the second lattice are shifted by vector $\mathbf{d} = (d_x, d_y)$ and, correspondingly, have the coordinates $\mathbf{r}_\mu^{(2)} = (ih_x + d_x, jh_y + d_y)$, and $\mathbf{h} = (h_x, h_y)$ is the interdipole distance in the sublattice. In our case of two embedded square lattices, we have $d_x = d_y = h_x/2 = h_y/2$. Let $\mathbf{M}_\mu^{(l)}(t) = \mathbf{M}(\mathbf{r}_\mu^{(l)}, t)$ be the magnetic moment of a dipole at point $\mathbf{r}_\mu^{(l)}$ and time t, where index $l = 1, 2$ designates the sublattice number. Here, the modulus of the magnetic moment in each sublattice is the same for all sites in the same sublattice ($M_\mu^{(l)}(t) = M^{(l)}$), and only a dipole direction can change from site to site.

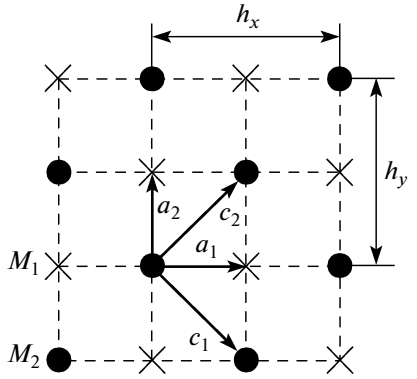

Fig. 2. Translation vectors of the total ($a_1 = (1, 0)$, $a_2 = (0, 1)$) and rotated ($c_1 = (\sqrt{2}, \sqrt{2})$, $c_2 = (\sqrt{2}, -\sqrt{2})$) square lattices. Crosses and dark points indicate the sites of sublattices M_1 and M_2, respectively.

The magnetic states of the lattice of isotropic dipoles were simulated using the SIMMAG software package [18]. The simulation is based on a numerical solution of a set of the Landau–Lifshitz equations

$$\frac{\partial \mathbf{M}_\mu^{(l)}(t)}{\partial t} = -\frac{\gamma}{1+\alpha^2}[\mathbf{M}_\mu^{(l)}(\mathbf{r}, t) \times \mathbf{H}_\mu^{(l)}(t)] - \frac{\gamma\alpha}{(1+\alpha^2)M^{(l)}} \times [\mathbf{M}_\mu^{(l)}(\mathbf{r}, t) \times [\mathbf{M}_\mu^{(l)}(\mathbf{r}, t) \times \mathbf{H}_\mu^{(l)}(t)]], \quad (1)$$

where γ is the gyromagnetic ratio, α is the dimensionless attenuation parameter, and $\mathbf{H}_\mu^{(l)}(t) = \mathbf{H}(\mathbf{r}_\mu^{(l)}, t)$ is the effective magnetic field at point $\mathbf{r}_\mu^{(l)}$ and time t. In our calculations, we took $\gamma = 1.76 \times 10^7$ Oe^{-1} s^{-1} and $\alpha = 1$. At zero temperature, the effective magnetic field is represented by dipole field $\mathbf{H}_D(\mathbf{r}, t)$, which can be calculated at any lattice site. When the problem is solved at a finite temperature of the interaction of the

system with a thermostat, the contribution of an additional term in the form of random field $\mathbf{H}_T(\mathbf{r}, t)$ to the effective magnetic field is simulated [19]. Thermal noise is delta-correlated in time and space,

$$\begin{aligned}&\langle \mathbf{H}_T(\mathbf{r}_\mu^{(l)}, t_1), \mathbf{H}_T(\mathbf{r}_\nu^{(l)}, t_2)\rangle \\ &= \sigma_l^2 \delta(t_1 - t_2)\delta(\mathbf{r}_\mu^{(l)} - \mathbf{r}_\nu^{(l)}),\end{aligned} \tag{2}$$

where $\sigma_l^2 = 2\alpha kT/\gamma M^{(l)}$ is the Boltzmann constant, and T is the temperature; the field has the form (see, e.g., [19])

$$\mathbf{H}_T(\mathbf{r}, t) = \frac{\sigma_l}{\sqrt{\Delta t}}\xi(\mathbf{r}, t), \tag{3}$$

where $\xi(\mathbf{r}, t)$ is the random quantity having a normal distribution with zero mean and unit variance and Δt is the time step of the numerical integration of the Landau–Lifshitz equation.

The field creating by all dipoles at point $\mathbf{r}_\mu$ has the form

$$\begin{aligned}\mathbf{H}_m(\mathbf{r}_\mu^{(l)}, t) &= \sum_\nu \hat{\mathbf{D}}(\mathbf{r}_\mu^{(l)} - \mathbf{r}_\nu^{(l)})\mathbf{M}_\nu^{(l)}(t) \\ &+ \sum_\nu \hat{\mathbf{D}}(\mathbf{r}_\mu^{(l)} - \mathbf{r}_\nu^{(n)} + \mathbf{d})\mathbf{M}_\nu^{(n)}(t), \\ l &= 1, 2, \quad n \neq l,\end{aligned} \tag{4}$$

where $\hat{\mathbf{D}}(\mathbf{r})$ is the dipole matrix, and the first and second terms in the right-hand side of Eq. (4) describe the magnetic fields that are responsible for the interaction of dipoles inside one sublattice and between the sublattices, respectively. Since it is impossible to perform a numerical simulation of arbitrary magnetic moment distributions over an infinite lattice, we consider periodic distributions of magnetic moment $\mathbf{M}_\mu^{(l)}(t)$ with period vector $\mathbf{N} = (N_x, N_y)$ so that

$$\mathbf{M}_\mu^{(l)}(t) = \mathbf{M}_{\mu + \hat{\mathbf{n}}\mathbf{N}}^{(l)}(t), \quad \hat{\mathbf{n}} = \begin{pmatrix} n_x & 0 \\ 0 & n_y \end{pmatrix},$$

where n_x and n_y are integers. Note that our numerical simulations show that the result is independent of the period at $N > 10$. In this case, the magnetostatic field can be represented as

$$\begin{aligned}\mathbf{H}_m(\mathbf{r}_\mu^{(l)}, t) &= \sum_{\nu=0}^{N-1} \hat{\mathbf{D}}^\infty(\mathbf{r}_\mu^{(l)} - \mathbf{r}_\nu^{(l)})\mathbf{M}_\nu^{(l)}(t) \\ &+ \sum_{\nu=0}^{N-1} \hat{\mathbf{D}}^\infty(\mathbf{r}_\mu^{(l)} - \mathbf{r}_\nu^{(n)} + \mathbf{d})\mathbf{M}_\nu^{(n)}(t),\end{aligned} \tag{5}$$

where

$$\hat{\mathbf{D}}^\infty(\mathbf{r}) = \sum_n \hat{\mathbf{D}}(\mathbf{r} + \mathbf{p}), \quad \mathbf{p} = (n_x N_x h_x, n_y N_y h_y).$$

Note that matrix $\hat{\mathbf{D}}^\infty(\mathbf{r})$ is periodic with period N. When calculating this matrix, we replaced an infinite sum by a finite one by choosing the number of terms so that the energy system was independent of this number. A similar procedure was applied in [20]. In our calculations, we restricted ourselves to 64 terms in the sum.

It is convenient to calculate the magnetostatic field using the fast Fourier transform. In this case, the field can be represented as

$$\begin{aligned}\mathbf{H}(\mathbf{r}_\mu^{(l)}, t) &= \frac{1}{N_x N_y}\sum_{\mathbf{q}} (\hat{\mathbf{M}}^{(l)}(\mathbf{q}, t)\hat{\hat{\mathbf{D}}}^\infty(\mathbf{q}) \\ &+ \hat{\mathbf{M}}^{(n)}(\mathbf{q}, t)\hat{\hat{\mathbf{D}}}_d^\infty(\mathbf{q})\exp(i(\mathbf{q}\cdot\mathbf{r}_\mu))),\end{aligned} \tag{6}$$

where $\hat{\hat{\mathbf{D}}}^\infty(\mathbf{q})$ and $\hat{\hat{\mathbf{D}}}_q^\infty(\mathbf{q})$ are the Fourier transforms of the total dipole matrices and $\hat{\mathbf{M}}^{(l)}(\mathbf{q})$ are the Fourier transforms for the distribution of the magnetic moments in the system. We have

$$\begin{aligned}\hat{\hat{\mathbf{D}}}^\infty(\mathbf{q}) &= \sum_{\mathbf{r}} \hat{\mathbf{D}}^\infty(\mathbf{r})\exp(-i(\mathbf{q}\cdot\mathbf{r})), \\ \hat{\hat{\mathbf{D}}}_d^\infty(\mathbf{q}) &= \sum_{\mathbf{r}} \hat{\mathbf{D}}^\infty(\mathbf{r} + \mathbf{d})\exp(-i(\mathbf{q}\cdot\mathbf{r})),\end{aligned} \tag{7}$$

$$\mathbf{M}_\mu^{(l)}(t) = \frac{1}{N_x N_y}\sum_{\mathbf{q}} \hat{\mathbf{M}}^{(l)}(\mathbf{q}, t)\exp(i(\mathbf{q}\cdot\mathbf{r}_\mu)), \tag{8}$$

$$\mathbf{M}^{(l)}(\mathbf{q}, t) = \sum_{\mathbf{r}_\mu} \hat{\mathbf{M}}_\mu^{(l)}(t)\exp(-i(\mathbf{q}\cdot\mathbf{r}_\mu)), \tag{9}$$

where $\mathbf{r}_\mu$ changes within the period of the magnetic moment distribution.

Thus, the calculation of the magnetostatic field of two embedded rectangular lattices of dipoles is reduced to a single computation of the Fourier transforms of total dipole matrices $\hat{\mathbf{D}}^\infty(\mathbf{r})$ and $\hat{\mathbf{D}}^\infty(\mathbf{r} + \mathbf{d})$, the computation of the Fourier transform of the magnetic moments, the multiplication of the obtained Fourier transforms, and the computation of the inverse Fourier transform. This procedure significantly accelerates the calculations.

The major portion of the numerical simulation was executed for a system of periodic distribution with a period of 10×10 cells, with each of which containing two different dipoles. The first sublattice contained dipoles with a magnetic moment of 4.2×10^{-18} erg/G, which approximately corresponded to the magnetic moment of a particle 1 nm in radius with a magnetization of 1000 G. The magnetic moments of the dipoles located in the second sublattice were changed from 4.2×10^{-18} erg/G to zero, which corresponded to the variation of δ from zero to unity. The dipoles were

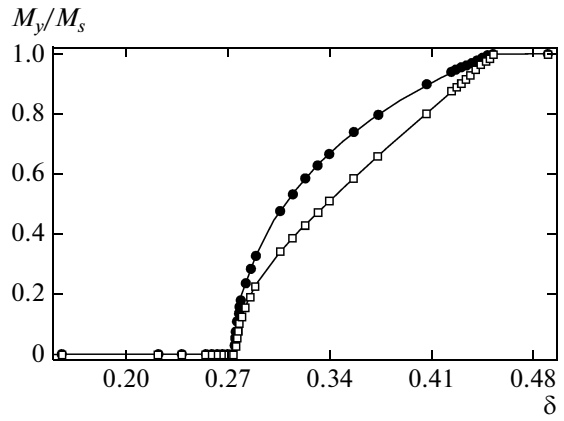

Fig. 3. Curve M_y/M_s describing the average normalized ferromagnetic moment of a sublattice at the values of δ corresponding to antiferromagnetic, noncollinear, and ferromagnetic states: (round and square symbols) numerical simulation data for large and small dipoles, respectively; (solid lines) corresponding analytical relations obtained using trial functions.

assumed to be isotropic. The interdipole distance in the sublattice was $h_x = h_y = 2$ nm. The sites of the second square lattice were placed exactly at the centers of the cells of the first sublattice. We studied the configurations of magnetic moments that correspond to the ground states over the entire δ range.

The algorithm of simulating the magnetic moment distribution in the system was as follows. The system is relaxed to a ground antiferromagnetic state starting from a random distribution of magnetic moments over the sublattices at $\delta = 0$. The system then passed through the entire chain of ground states in the range $\delta = 0$–1 when the mismatch of magnetic moments δ was changed and relaxation was performed at each step. The calculations were carried out at a finite amplitude of the thermal field corresponding to a temperature $T = 0.01$–0.05 K for a perturbation to be introduced into the system and a magnetic moment distribution to be restructured when parameter δ was changed. The state energy was calculated at zero temperature.

Figure 1 shows stationary magnetic moment distributions at various values of mismatch parameter δ. The simulation showed that the states of the system at various values of mismatch δ are independent of both period $\mathbf{N} = (N_x, N_y)$ and the sublattice step.

In the case of $\delta = 0$, the magnetic moments of the dipoles from different sublattices are the same, and the system represents a simple square lattice of identical dipoles. In the case of zero temperature, the initial random distribution of dipoles relaxes into the microvortex state that is degenerate in the angle between magnetic moments and the lattice axes (Fig. 1a), which completely agrees with the well-known data in [4]. When a finite temperature is "turned on," the system transforms into an antiferromagnetic state, where dipoles are arranged along the side of the "dense" square lattice (Fig. 1b). Note that this antiferromagnetic state is a particular case of the microvortex state [1, 4]. The splitting of the microvortex state because of thermal fluctuations and the transition of the system into an antiferromagnetic state were predicted in [15, 21] and explained by the fact that the spectrum of spin-wave fluctuations near the ground state $\lambda(\mathbf{k})$ depends on microvortex angle φ. As a result, the corresponding contribution to the free energy of the system is also a function of angle φ, and its maximum is reached exactly in the antiferromagnetic ordering of dipoles. Thus, our numerical model adequately describes this phenomenon.

As mismatch δ increases, the antiferromagnetic state remains stable up to a critical value $\delta_{c1} = 0.27$. When this critical value is exceeded, a state that can be called noncollinear appears, since the angles of deviation are different for the sublattices of "large" and "small" dipoles (Fig. 1c). Figure 3 shows the appearing perpendicular components of the magnetic moments versus the mismatch parameter. In essence, the transition consists in the fact that a ferromagnetic moment with an average magnetization directed normal to the initial direction of magnetic dipoles appears in the system against the background of antiferromagnetism. This phase transition substantially resembles the topological spin-flop transition that is observed in an external magnetic field during a numerical simulation of a system of magnetic dipoles with an in-plane magnetization and a rather weak anisotropy in the basal plane [22].

This phase transition is a second-order phase transition, and the order parameter is represented by the component of the average magnetic moment of the sublattice directed normal to the antiferromagnetism vector in the initial antiferromagnetic state. The phase transition is characterized by critical behavior of the type $M_y \approx (\delta - \delta_c)^\nu$, $\delta_c = \delta_{c1}$. The analytical curve calculated by the trial function method (see Section 3) and the data obtained in a numerical experiment give a critical index $\nu = 1/2$ (Fig. 3). The values of the critical index coincide for both sublattices.

As the mismatch between the magnetic moments of the sublattices increases, the angles of deviation increase and the system transforms into a ferromagnetic state at the second critical value ($\delta_{c2} = 0.45$). At zero temperature, this state is uniformly angle degenerate and a numerical calculation gives the same energies of the system irrespective of the magnetization direction of the system. Nevertheless, the ferromagnetic state in which all dipoles are directed along the diagonal of the sublattices normal to the antiferromagnetism vector in the initial ferromagnetic state at $\delta = 0$ always forms at zero temperature in a numerical experiment at $\delta < 0.659$ (Fig. 1d). This unambiguous selection of the magnetization direction in the ferromagnetic state is likely to be related to the splitting of the ground state because of thermal spin-wave fluctu-

ations, similarly to the case of the ground microvortex state at $\delta = 0$ [15, 21]. At $\delta > \delta_{c3} = 0.673$, the state remains antiferromagnetic but the dipoles rotate through an angle of 45° and are oriented along the cell side in the square sublattice (Fig. 1e). This behavior is associated with the fact that, as δ increases, the free energy of the state with dipoles oriented along the side of the square cell becomes lower than the free energy of the state with dipoles oriented along its diagonal. In the range $0.659 < \delta < 0.673$, the free energies of all ferromagnetic states are close to each other and the relaxation times increase even at a nonzero temperature, which makes it impossible to find the boundary between the two ferromagnetic states under study more exactly under numerical experiment conditions. As the mismatch parameter increases further, the ferromagnetic state remains stable up to $\delta_{c4} = 0.868$.

In the range $0.868 < \delta < 1$, a parquet-like configuration of magnetic dipoles forms (Fig. 1f). It is characterized by the fact that the initial ferromagnetic ordering is retained in the small-dipole sublattice and that an "antiferromagnetic" order with a perpendicularly directed antiferromagnetism vector appears in the large-dipole sublattice against the background of the retained ferromagnetic ordering. A numerical simulation shows a linear relation between the average magnetization of the large-spin sublattice and parameter δ over the entire range of this phase (Fig. 4). As δ increases, large dipoles rotate in an antiferromagnetic manner more intensely. In this case, the order parameter is represented by the antiferromagnetism vector appearing the large-spin sublattice. A numerical simulation gives the relation $L \approx (\delta - \delta_{c4})^{0.5}$ for this order parameter; that is, the critical index is 1/2. At $\delta = \delta_{c5} = 1$ (where the value of the small dipoles becomes zero), the large-dipole sublattice reaches the ideal antiferromagnetic ordering that should take place in a simple square lattice (Fig. 1g). In this case, the order parameter is represented by the ferromagnetic component of the average magnetic moment of the large-dipole sublattice. Since it linearly depends on δ, the critical index at the phase-transition point at $\delta = \delta_{c5} = 1$ is 1. Both phase transitions at $d = \delta_{c4} = 0.868$ and $\delta = \delta_{c5} = 1$ are second-order phase transitions.

3. DISCUSSION

The character of the orientation ordering of a dipole system in the ground state is determined by the minimum of the magnetostatic dipole–dipole interaction energy

$$E = \sum_{\mathbf{R} \neq \mathbf{R}'} \mathbf{D}_{ik}(\mathbf{R} - \mathbf{R}') M_i(\mathbf{R}) M_k(\mathbf{R}'). \qquad (10)$$

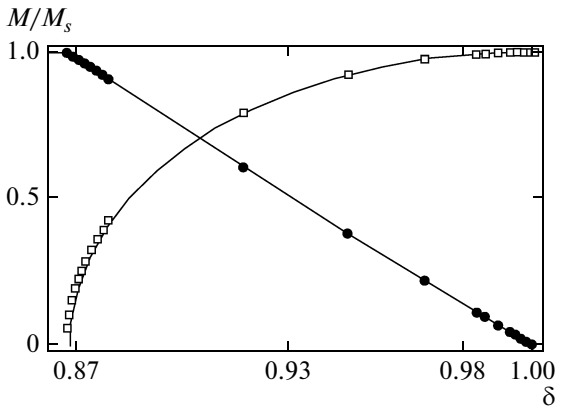

Fig. 4. Average (●) ferromagnetic and (□) antiferromagnetic moments of the large-dipole sublattice in a parquet configuration that were obtained during numerical simulation: (solid lines) corresponding analytical relations found using trial functions.

In the dipole approximation, the components of the magnetostatic interaction tensor are

$$D_{ik}(\mathbf{r}) = \frac{\delta_{ik}}{r^3} - 3\frac{\mathbf{r}_i \cdot \mathbf{r}_k}{r^5}, \qquad (11)$$

and subscripts $i, k = x, y$ number the Cartesian coordinate axes. We also determine the Fourier transforms of magnetostatic tensor components (11),

$$S_{ik}(\mathbf{k}) = \sum_{\mathbf{r} \neq 0} D_{ik}(\mathbf{r}) \exp(i\mathbf{k} \cdot \mathbf{r}).$$

Vector $\mathbf{M}$ changes according to the law $|\mathbf{M}| = M(1 + \delta \exp(i\mathbf{b} \cdot \mathbf{R}))$, where $M = (M^{(1)} + M^{(2)})/2$ is the average magnetic moment of two dipoles in the unit cell, $\mathbf{R} = n\mathbf{a}_1 + l\mathbf{a}_2$ ($n, l = 0, \pm 1, \ldots$) are two-dimensional lattice sites, $\mathbf{b} = \mathbf{b}_1 + \mathbf{b}_2$ is the reciprocal lattice vector that meets the condition $\mathbf{b}_i \cdot \mathbf{a}_k = \pi\delta_{ik}$, and δ_{ik} is the Kronecker delta.

The expression for the energy acquires the form

$$E = M^2 \sum_{\mathbf{R} \neq \mathbf{R}'} [1 + \delta(\exp(i\mathbf{b} \cdot \mathbf{R}) + \exp(i\mathbf{b} \cdot \mathbf{R}')) + \delta^2 \exp(i\mathbf{b} \cdot (\mathbf{R} - \mathbf{R}')) D_{ik}(\mathbf{R} - \mathbf{R}')] \times \mathbf{m}_i(\mathbf{R}) \cdot \mathbf{m}_k(\mathbf{R}'), \qquad (12)$$

where the dipole orientation is described by two-dimensional vectors $\mathbf{m}(\mathbf{R})$, which lie in the lattice plane and meet the normalization condition $\mathbf{m}^2(\mathbf{R}) = 1$. The numerical simulation data can be used to choose relatively simple trial functions and to analyze the phase transitions occurring over the entire δ range. Any of the states observed in the numerical experiment can be

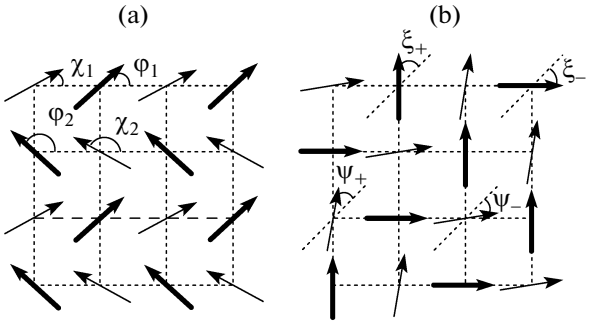

Fig. 5. Sequential noncollinear states that occur on a square lattice when the mismatch between the dipole moments increases.

described using a four-sublattice trial function, which has the following form for states (a)–(c) in Fig. 1:

$$\mathbf{m}(\mathbf{R}) = \frac{1+\cos(\mathbf{b}_2\cdot\mathbf{R})}{2}\left(\frac{1+\cos(\mathbf{b}_1\cdot\mathbf{R})}{2}\mathbf{d}_1 + \frac{1-\cos(\mathbf{b}_1\cdot\mathbf{R})}{2}\mathbf{e}_1\right) + \frac{1-\cos(\mathbf{b}_2\cdot\mathbf{R})}{2} \times\left(\frac{1+\cos(\mathbf{b}_1\cdot\mathbf{R})}{2}\mathbf{e}_2 + \frac{1-\cos(\mathbf{b}_1\cdot\mathbf{R})}{2}\mathbf{d}_2\right). \quad (13)$$

Unit vectors $\mathbf{d}_j$ and $\mathbf{e}_j$ are directed along the magnetic moments of large and small dipoles, respectively, the orientations of which are designated by angles φ_j and χ_j and subscript $j = 1, 2$ indicates the magnetic sublattice number (Fig. 5a)

$$\mathbf{d}_j = \{\cos\chi_j, \sin\chi_j\}, \quad \mathbf{e}_j = \{\cos\varphi_j, \sin\varphi_j\}. \quad (14)$$

States (f)–(h) in Fig. 1 can be described by another trial function with the following set of sublattices (Fig. 5b):

$$\mathbf{m}(\mathbf{R}) = \sin\left(\frac{\mathbf{b}\cdot\mathbf{R}}{2}\right)\left(\frac{1+\sin(\mathbf{b}\cdot\mathbf{R})/2}{2}\mathbf{e}_+ - \frac{1-\sin(\mathbf{b}\cdot\mathbf{R})/2}{2}\mathbf{e}_-\right) + \cos\left(\frac{\mathbf{b}\cdot\mathbf{R}}{2}\right) \times\left(\frac{1+\cos(\mathbf{b}\cdot\mathbf{R})/2}{2}\mathbf{d}_+ - \frac{1-\cos(\mathbf{b}\cdot\mathbf{R})/2}{2}\mathbf{d}_-\right). \quad (15)$$

The orientations of the unit vectors along the sublattice magnetizations are determined by angles $\psi_\pm$ and $\xi_\pm$ for large and small dipoles, respectively (Fig. 5b),

$$\mathbf{d}_\pm = \{\cos(\pi/4 \pm \xi_\pm), \sin(\pi/4 \pm \xi_\pm)\}, \quad \mathbf{e}_\pm = \{\cos(\pi/4 \pm \psi_\pm), \sin(\pi/4 \pm \psi_\pm)\}. \quad (16)$$

States (d) and (e) in Fig. 1 can be described by any of these functions due to their higher symmetry. The symmetry of the magnetization distribution in the detected states makes it possible to introduce additional relations for the values of angles φ_j, χ_j, $\psi_\pm$, and $\xi_\pm$ given in the table. Note that trial function (13) contains the microvortex solution (Fig. 1a), which corresponds to a set of parameters $\chi_1 = -\varphi_1$, $\varphi_2 = \varphi_1 + \pi$, and $\chi_2 = \chi_1 + \pi$ and a ferromagnetic phase degenerating with respect to the orientation to the crystallographic axes in a continuous manner. The parquet state is described by the introduction of the following three sublattices: a sublattice uniformly magnetized along the diagonal of the small-dipole sublattice and two canted large-dipole sublattices embedded into each other at angle 2ξ between the magnetic moment directions.

The minimization of the system energy using trial functions (13) (calculation system is described in detail in Appendix) leads to root dependences of variational parameters $\varphi(\delta)$ and $\chi(\delta)$ near the point of the phase transition from the antiferromagnetic into the noncollinear state, $\varphi = \varphi_0(\delta_{c1})\sqrt{\delta - \delta_{c1}}$ and $\chi = \chi_0(\delta_{c1})\sqrt{\delta - \delta_{c1}}$. The expressions for φ_0 and χ_0 are combinations of the magnetostatic tensor components at the symmetric points of the Brillouin zone and are

Angles $\varphi_{1,2}$, $\chi_{1,2}$, $\psi_\pm$, and $\xi_\pm$ corresponding to various magnetic distributions

	φ_1	φ_2	χ_1	χ_2	ψ_+	ψ_-	ξ_+	ξ_-
Microvortex (Fig. 1a)	φ	$\pi+\varphi$	$-\varphi$	$\pi-\varphi$	–	–	–	–
Antiferromagnetic at $\delta = 0$ (Fig. 1b)	π	0	π	0	–	–	–	–
Noncollinear (Fig. 1c)	$\pi-\varphi$	φ	$\pi-\chi$	χ	–	–	–	–
1st ferromagnetic (Fig. 1d)	$\frac{\pi}{2}$	$\frac{\pi}{2}$	$\frac{\pi}{2}$	$\frac{\pi}{2}$	$\frac{\pi}{4}$	$-\frac{\pi}{4}$	$\frac{\pi}{4}$	$-\frac{\pi}{4}$
2nd ferromagnetic (Fig. 1e)	$\frac{\pi}{4}$	$\frac{\pi}{4}$	$\frac{\pi}{4}$	$\frac{\pi}{4}$	0	0	0	0
Parquet (Fig. 1f)	–	–	–	–	0	0	ξ	ξ
Antiferromagnetic (Fig. 1g)	–	–	–	–	–	–	$\frac{\pi}{2}$	$\frac{\pi}{2}$

awkward. We do not write them explicitly here and only present their calculated values corresponding to the energy minimum, $\varphi_0 \approx 2.7848$ and $\chi_0 \approx 1.8519$. The critical value of mismatch parameter δ_{c1} at which the antiferromagnetic ordering is broken has the form

$$\delta_{c1}^2 = \frac{(S(0) - S(\mathbf{b}_1))(S(\mathbf{b}) - S(\mathbf{b}_1))}{(S(0) - S(\mathbf{b}_2))(S(\mathbf{b}) - S(\mathbf{b}_2))}. \quad (17)$$

At the symmetric points of the Brillouin zone, we have $S_{xx}(0) = S_{yy}(0) \equiv S(0)$, $S_{xx}(\mathbf{b}) = S_{yy}(\mathbf{b}) \equiv S(\mathbf{b})$, $S_{xx}(\mathbf{b}_1) = S_{yy}(\mathbf{b}_2) \equiv S(\mathbf{b}_2)$, and $S_{xx}(\mathbf{b}_2) = S_{yy}(\mathbf{b}_1) \equiv S(\mathbf{b}_1)$ for the Fourier transforms of the magnetostatic tensor components.

In the dipole approximation ($S(0) \approx -4.5168$, $S(\mathbf{b}) \approx 1.3229$, $S(\mathbf{b}_1) \approx -5.0989$, $S(\mathbf{b}_2) \approx 6.0343$ [1, 4]), we obtain $\delta_{c1} \approx 0.2742$. At $\delta > \delta_{c1} \approx 0.2742$, the antiferromagnetic structure begins to distort and a weak ferromagnetic order appears in the system.

The expansion of the system energy in the vicinity of the phase-transition point has the form

$$E \approx E_{AF} - \alpha(\delta_{c1})M^2(\delta - \delta_{c1})^2, \quad (18)$$

where

$$E_{AF} = \frac{M^2}{2}(S(\mathbf{b}) + \delta^2 S(\mathbf{b}_2))$$

is the energy of the antiferromagnetic ordering of magnetic moments. Coefficient α is estimated to be $\alpha \approx 6.0208$. Note that the behavior of energy (18) near critical parameter δ_{c1} corresponds to the criterion of second-order phase transitions.

When the mismatch between the magnetic moments of the sublattices increases gradually, the magnetic moments rotate so that the system transforms into a ferromagnetically ordered state at $\delta = \delta_{c2}$ (Fig. 1d). Here, we have

$$\delta_{c2}^2 = \frac{(S(0) - S(\mathbf{b}_1))(S(0) - S(\mathbf{b}_2))}{(S(\mathbf{b}) - S(\mathbf{b}_1))(S(\mathbf{b}) - S(\mathbf{b}_2))} \approx 0.4506. \quad (19)$$

In the vicinity of critical parameter $\delta = \delta_{c2}$, the canting angles are $\varphi = \pi/2 - \tilde{\varphi}$ and $\chi = \pi/2 - \tilde{\chi}$, where $\tilde{\varphi} = \varphi_1\sqrt{\delta_{c2} - \delta}$ and $\tilde{\chi} = \chi_1\sqrt{\delta_{c2} - \delta}$. The calculation of parameters φ_1 and χ_1 at which the energy is minimal results in the values $\varphi_1 \approx 1.9949$ and $\chi_1 \approx 2.9997$.

The expression for the energy near the transition into a homogeneous ferromagnetic state is also a quadratic function of deviation $\delta - \delta_{c2}$,

$$E \approx E_F - M^2\beta(\delta_{c2})(\delta - \delta_{c2})^2, \quad (20)$$

where E_F is the ferromagnetic state energy,

$$E_F = \frac{M^2}{2}(S(0) + \delta^2 S(\mathbf{b})).$$

Parameter β is calculated to be $\beta \approx 3.6632$. This phase transition is also a second-order phase transition.

It is well known that the character of ordering in two-dimensional magnetic dipole lattices is determined by the sign of interaction of two dipole chains. In the case where the chains consist of alternating dipoles of different values, the energy of their interaction depends on the mismatch between the magnetic moments and has the form $8\pi^2M^2\exp(-\pi)[\exp(-\pi) - \delta^2/2^{3/2}]$. Thus, the interaction energy changes its sign at $\delta = \delta_0 \approx 0.3496$; that is, the chains interact antiferromagnetically at $\delta < \delta_0$ and ferromagnetically at $\delta > \delta_0$. Obviously, noncollinear states cannot appear in the system of two chains under study; as a result, the antiferromagnetic ordering at $\delta = \delta_0$, where $\delta_{c1} < \delta_0 < \delta_{c2}$, transforms directly into a ferromagnetic order. It is obvious that the restructuring of the magnetic moments in a square lattice is related to a change in the character of the interchain interaction in the system. Indeed, large magnetic moments in the noncollinear state are rotated through a higher angle as compared to the initial antiferromagnetic state, whereas small magnetic moments are rotated through a lower angle (Fig. 3). Correspondingly, the mismatch between the projections of the magnetic moments of different sublattices onto the horizontal axis remains small (Fig. 1c), whereas the mismatch between the corresponding projections onto the vertical axis is substantially larger. Thus, antiferromagnetic interaction is retained between the horizontal dipole chains, while the interaction between the vertical chains is ferromagnetic. As a result, a noncollinear state becomes energetically favorable. It is interesting that the mismatches between the projections of the spins of different sublattices onto the vertical and horizontal axes, which are calculated as $\delta_x = (M_x^{(1)} - M_x^{(2)})/(M_x^{(1)} + M_x^{(2)})$ and $\delta_y = (M_y^{(1)} - M_y^{(2)})/(M_y^{(1)} + M_y^{(2)})$, remain constant over the entire δ range corresponding to the noncollinear phase and are $\delta_x = \delta_{c1} \approx 0.275$ and $\delta_y = \delta_{c2} \approx 0.452$. It is obvious that $\delta_x < \delta_0$ and $\delta_y > \delta_0$, which corresponds to an antiferromagnetic interaction between the horizontal chains and a ferromagnetic interaction between the vertical chains.

As discussed above, a further increase in parameter δ leads to the transformation of the system into a ferromagnetic state along the lattice diagonal. Then, the sublattice of the dipoles with a higher moment forms a structure consisting of two canted lattices inserted into each other at angle 2ξ between them, whereas the small dipoles retain ferromagnetic ordering (see Fig. 1f). When mismatch parameter δ exceeds the critical value $\delta \geq \delta_{c3}$, where

$$\delta_{c3} = \frac{S(\mathbf{b}/2) - S(0) - S_{xy}(\mathbf{b}/2)}{S(\mathbf{b}) - S(\mathbf{b}/2) + S_{xy}(\mathbf{b}/2)} \approx 0.8683, \quad (21)$$

variational parameter ξ, the cosine of which determines the unit vector along the ferromagnetism vector, is found from the expression

$$\cos\xi = \frac{S(\mathbf{b}) - S(0)}{S(0) + S(\mathbf{b}) - 2S(\mathbf{b}/2) + 2S_{xy}(\mathbf{b}/2)} \times \frac{1-\delta}{1+\delta} \approx 14.1887\frac{1-\delta}{1+\delta}. \quad (22)$$

In the vicinity of the phase-transition point, angle ξ obeys a root dependence on the distance from the critical point, which coincides with the numerical simulation data,

$$\xi \approx \frac{2}{1+\delta_{c3}}\sqrt{\frac{S(\mathbf{b}) - S(0)}{S(0) + S(\mathbf{b}) - 2S(\mathbf{b}/2) + 2S_{xy}(\mathbf{b}/2)}} \times \sqrt{\delta - \delta_{c3}} \approx 4.0323\sqrt{\delta - \delta_{c3}}.$$

The energy of the three-sublattice structure under study decreases with respect to uniform ordering and is

$$E = E_F - M^2\frac{(1+\delta)^2}{8}\left(S(0) + S(\mathbf{b}) - 2S\left(\frac{\mathbf{b}}{2}\right) + 2S_{xy}\left(\frac{\mathbf{b}}{2}\right)\right)(1-\cos\xi)^2. \quad (23)$$

When the value $\delta_{c4} = 1$ is reached, we pass to a simple square lattice of identical dipoles with an antiferromagnetic order, with the antiferromagnetism vector being oriented normal to the initial ferromagnetism vector.

Thus, we considered the system in which magnetic particles have different dipole moments and are arranged in a staggered order on a square lattice. Using a numerical simulation, we studied the change of the magnetic configurations in the system and the character of the phase transitions between them that are caused by a change in the mismatch between the dipoles. It was shown that all phase transitions between sequential collinear and noncollinear states are second-order phase transitions and that the behavior of the order parameters is described by relations of the type $\alpha\left|\tilde{\delta} - \delta_c\right|^{\nu}$, where coefficient α is a numerical constant and the critical index is $\nu = 1/2$. Note that the developed numerical model can be used to adequately simulate the fluctuation phase transition that removes the degeneracy of the ground microvortex state in a zero magnetic field and to predict a change in the orientation of the ferromagnetic ordering in a ferromagnetic phase, which is likely also to be related to a spin-wave contribution to the system energy at zero temperature. The numerical simulation results were supported by analytical computations using trial functions, and the calculated phase characteristics of the system agree very well with the numerical simulation results.

APPENDIX

Using the transition from an antiferromagnetic into a noncollinear state as an example, we describe a method for calculating the variational system parameter. Energy (12) written with trial functions (13) is written as

$$E = \frac{M^2}{8}(1+\delta^2)(S(0) + S(\mathbf{b}) + S(\mathbf{b}_1) + S(\mathbf{b}_2)) + \frac{M^2}{16}\{[(1+\delta)^2\cos(\varphi_1 - \varphi_2) + (1-\delta)^2\cos(\chi_1 - \chi_2)] \times (S(0) + S(\mathbf{b}) - S(\mathbf{b}_1) - S(\mathbf{b}_2)) + (1-\delta^2)[\cos(\varphi_1 - \chi_1) + \cos(\varphi_1 - \chi_2) + \cos(\varphi_2 - \chi_1) + \cos(\varphi_2 - \chi_2)](S(0) - S(\mathbf{b})) + (1-\delta^2)[\cos(\varphi_1 + \chi_1) - \cos(\varphi_1 + \chi_2) - \cos(\varphi_2 + \chi_1) + \cos(\varphi_2 + \chi_2)](S(\mathbf{b}_1) - S(\mathbf{b}_2))\}. \quad (24)$$

As the solution, we chose the function that describes the noncollinear state (see Fig. 1c). Owing to symmetry, we can choose two angles related as

$$\varphi_2 = \varphi, \quad \varphi_1 = \pi - \varphi, \quad (25)$$

$$\chi_2 = \chi, \quad \chi_1 = \pi - \chi \quad (26)$$

instead of four independent angles. Substituting Eqs. (25) and (26) into Eq. (24), we obtain the expression

$$E = \frac{M^2}{8}(1+\delta^2)(S(0) + S(\mathbf{b}) + S(\mathbf{b}_1) + S(\mathbf{b}_2)) + \frac{M^2}{16}\{-[(1+\delta)^2\cos(2\varphi) + (1-\delta)^2\cos(2\chi)] \times (S(0) + S(\mathbf{b}) - S(\mathbf{b}_1) - S(\mathbf{b}_2)) + 2(1-\delta^2) \times \cos(\chi - \varphi)(S(0) - S(\mathbf{b}) + S(\mathbf{b}_1) - S(\mathbf{b}_2)) - 2(1-\delta^2) \times \cos(\chi + \varphi)(S(0) - S(\mathbf{b}) - S(\mathbf{b}_1) + S(\mathbf{b}_2))\} \quad (27)$$

to determine the values of variational parameters χ and φ from its minimum. At low values of parameter δ, an antiferromagnetic state ($\varphi = \chi = 0$) corresponds to the minimum of energy (27). The condition of stability of this state is a positive value of the quantity

$$\Delta_{AF} = \left(\frac{\partial^2 E}{\partial\varphi^2}\frac{\partial^2 E}{\partial\chi^2} - \left(\frac{\partial^2 E}{\partial\varphi\partial\chi}\right)^2\right)\Bigg|_{\varphi=0;\,\chi=0} = \frac{M^2}{4}(1-\delta^2)[(S(0) - S(\mathbf{b}_1))(S(\mathbf{b}) - S(\mathbf{b}_1)) - \delta^2(S(0) - S(\mathbf{b}_2))(S(\mathbf{b}) - S(\mathbf{b}_2))]. \quad (28)$$

Correspondingly, the critical value of mismatch parameter δ_{c1} at which the antiferromagnetic ordering is broken is

$$\delta_{c1}^2 = \frac{(S(0) - S(\mathbf{b}_1))(S(\mathbf{b}) - S(\mathbf{b}_1))}{(S(0) - S(\mathbf{b}_2))(S(\mathbf{b}) - S(\mathbf{b}_2))}, \quad (29)$$

from which we have $\delta_{c1} \approx 0.2742$. When expanding Eq. (28) in the first order near the phase-transition point ($\delta \approx \delta_{c1}$), we obtain

$$\Delta_{AF} \approx \Delta_{AF0}(\delta_{c1})(\delta_{c1} - \delta), \tag{30}$$

where

$$\Delta_{AF0}(\delta_{c1}) = \frac{M^4}{2}\delta_{c1}(1-\delta_{c1}^2) \times (S(0) - S(\mathbf{b}_2))(S(\mathbf{b}) - S(\mathbf{b}_2)).$$

Obviously, the ratio Δ_{AF}/Δ_{AF0} plays the role of temperature in the theory of phase transitions and characterizes the closeness to the critical point. At $\delta > \delta_{c1} \approx 0.2742$, the antiferromagnetic structure begins to distort and a weak ferromagnetic order appears in the system.

In the first order in parameter Δ_{AF}, the behavior of functions $\varphi(\delta)$ and $\chi(\delta)$ near the transition point is described by the set of equations

$$\begin{cases} \dfrac{\partial E}{\partial \varphi} = 0, \\ \dfrac{\partial E}{\partial \chi} = 0, \end{cases}$$

which can be reduced to the form

$$\begin{aligned} 8\delta\Delta_{AF}\varphi &= (A_{AF} - B_{AF})(\varphi^2 - \chi^2) \\ &\times (B_{AF}(1+\delta)^2\varphi + C_{AF}(1-\delta)^2\chi), \\ 8\delta\Delta_{AF}\chi &= (A_{AF} - B_{AF})(\chi^2 - \varphi^2) \\ &\times (C_{AF}(1+\delta)^2\varphi + A_{AF}(1-\delta)^2\chi), \end{aligned} \tag{31}$$

where A_{AF}, B_{AF}, and C_{AF} are the second partial derivatives of the energy with respect to parameters φ and χ that are calculated at the point of antiferromagnetic ordering,

$$A_{AF} = \left.\frac{\partial^2 E}{\partial \varphi^2}\right|_{\varphi=0,\chi=0}, \quad B_{AF} = \left.\frac{\partial^2 E}{\partial \chi^2}\right|_{\varphi=0,\chi=0},$$
$$C_{AF} = \left.\frac{\partial^2 E}{\partial \varphi \partial \chi}\right|_{\varphi=0,\chi=0}.$$

Since $\Delta_{AF} \sim \delta_{c1} - \delta$ near the transition, we assume $\delta = \delta_{c1}$ and search for the solution to set (31) in the form $\varphi = \varphi_0(\delta_{c1})\sqrt{\delta - \delta_{c1}}$ and $\chi = \chi_0(\delta_{c1})\sqrt{\delta - \delta_{c1}}$. The expressions for φ_0 and χ_0 are combinations of the magnetostatic tensor components at the symmetric points of the Brillouin zone and are awkward. We do not write them explicitly here and only present their numerical estimates corresponding to the energy minimum, $\varphi_0 \approx 2.7848$ and $\chi_0 \approx 1.8519$.

To reveal the character of the transition, we expand energy (27) at the vicinity of the phase-transition point with allowance for set (31),

$$\begin{aligned} E \approx E_{AF} &+ \left(\frac{3}{4}\frac{(1+\delta)^2}{\delta}(A_{AF} - B_{AF}) - A_{AF}\right)\frac{\varphi^4}{24} \\ &+ \left(\frac{3}{4}\frac{(1-\delta)^2}{\delta}(A_{AF} - B_{AF}) - B_{AF}\right)\frac{\chi^4}{24} \\ &- \frac{A_{AF}(1+\delta)^2 - B_{AF}(1-\delta)^2}{16\delta}\varphi^2\chi^2 \\ &- C_{AF}\frac{\varphi^2 + \chi^2}{6}\varphi\chi. \end{aligned} \tag{32}$$

Here,

$$E_{AF} = \frac{M^2}{2}(S(\mathbf{b}_1) + \delta^2 S(\mathbf{b}_2))$$

is the energy of the antiferromagnetic ordering of the magnetic moments. Using the shape of the $\varphi(\delta)$ and $\chi(\delta)$ curves near δ_{c1}, we can write the energy in the form

$$E \approx E_{AF} - \alpha(\delta_{c1})M^2(\delta - \delta_{c1})^2. \tag{33}$$

Coefficient α is calculated to be $\alpha \approx 6.0208$. Note that the form of energy (32) corresponds to the criterion of second-order phase transitions.

ACKNOWLEDGMENTS

This work was supported by the Russian Foundation for Basic Research (project nos. 11-02-00434-a, 12-02-00988-a), the Ministry of Education and Science of the Russian Federation (project nos. 8565, 8750), and foundation Dinastiya of noncommercial programs.

REFERENCES

1. V. M. Rozenbaum, V. M. Ogenko, and A. A. Chuiko, Sov. Phys.—Usp. **34** (10), 883 (1991).
2. V. M. Rozenbaum, Sov. Phys. JETP **72** (6), 1028 (1991).
3. V. M. Rozenbaum, Phys. Rev. B: Condens. Matter **51**, 1290 (1995).
4. P. I. Belobrov, R. S. Gekht, and V. A. Ignatchenko, Sov. Phys. JETP **57** (3), 636 (1983).
5. A. A. Fraerman and M. V. Sapozhnikov, J. Magn. Magn. Mater. **192**, 191 (1999).
6. E. Z. Meilikhov and R. M. Farzetdinova, J. Exp. Theor. Phys. **94** (4), 751 (2002).
7. A. Yu. Galkin, B. A. Ivanov, and A. Yu. Merkulov, J. Exp. Theor. Phys. **101** (6), 1106 (2005).
8. J. E. L. Bishop, A. Yu. Galkin, and B. A. Ivanov, Phys. Rev. B: Condens. Matter **65**, 174403 (2002).
9. A. A. Fraerman, S. A. Gusev, L. A. Mazo, I. M. Nefedov, Yu. N. Nozdrin, I. R. Karetnikova, M. V. Sapozhnikov, I. A. Shereshevskii, and L. V. Sukhodoev, Phys. Rev. B: Condens. Matter **65**, 064424 (2002).

10. M. Ewerlin, D. Demirbas, F. Br ussing, O. Petracic, A.Ünal, S. Valencia, F. Kronast, and H. Zabel, Phys. Rev. Lett. **110**, 177209 (2013).
11. N. Mikuszeit, L. Baraban, E. Y. Vedmedenko, A. Erbe, P. Leiderer, and R. Wiesendanger, Phys. Rev. B: Condens. Matter **80**, 014402 (2009).
12. V. Novosad, K. Yu. Guslienko, H. Shima, Y. Otani, S. G. Kim, K. Fukamichi, N. Kikuchi, O. Kitakami, and Y. Shimada, Phys. Rev. B: Condens. Matter **65**, 060402(R) (2002).
13. Hyuk-Jae Jang, Pete Eames, E. Dan Dahlberg, M. Farhoud, and C. A. Ross, Appl. Phys. Lett. **86**, 023102 (2005).
14. R. P. Cowburn, A. O. Adeyeye, and M. E. Welland, New J. Phys. **1**, 6.1 (1999).
15. S. Prakash and C. L. Henley, Phys. Rev. B: Condens. Matter **42**, 6574 (1990).
16. C. Nisoli, R. Moessner, and P. Schiffer, Rev. Mod. Phys. **85**, 1473 (2013).
17. K. R. Mukhamatchin and A. A. Fraerman, JETP Lett. **93** (12), 716 (2011).
18. I. M. Nefedov, I. R. Karetnikova, and I. A. Shereshevskii, in *Proceedings of the XII International Symposium "Nanophysics and Nanoelectronics," Institute for Physics of Microstructures, Russian Academy of Sciences, Nizhni Novgorod, Russia, March 10–14, 2008* (Nizhni Novgorod, 2008), Vol. 2, p. 277.
19. I. R. Karetnikova, I. M. Nefedov, M. V. Sapozhnikov, A. A. Fraerman, and I. A. Shereshevskii, Phys. Solid State **43** (11), 2115 (2001).
20. K. M. Lelecki, M. J. Donahue, and M. W. Gutowski, J. Phys. D: Appl. Phys. **41**, 175005 (2008).
21. V. M. Rozenbaum, J. Exp. Theor. Phys. **84** (2), 368 (1997).
22. A. Yu. Galkin and B. A. Ivanov, JETP Lett. **83** (9), 383 (2006).

Translated by K. Shakhlevich